Hadronic Production of S-wave and P-wave Charmed Beauty Mesons via Heavy Quark Fragmentation

Kingman Cheung*

Center for Particle Physics, University of Texas at Austin, Austin TX 78712 U.S.A.

Tzu Chiang Yuan [†]

Davis Institute for High Energy Physics, Department of Physics,

University of California at Davis, Davis CA 95616 U.S.A.

Abstract

At hadron colliders the dominant production mechanism of $(\bar{b}c)$ mesons with large transverse momentum is due to parton fragmentation. We compute in a model-independent way the production rates and transverse momentum spectra for S-wave and P-wave $(\bar{b}c)$ mesons at the Tevatron via the direct fragmentation of the bottom antiquark as well as the Altarelli-Parisi induced gluon fragmentation. Since all the radially and orbitally excited $(\bar{b}c)$ mesons below the BD flavor threshold will cascade into the pseudoscalar ground state B_c through electromagnetic and/or hadronic transitions, they all contribute to the inclusive production of B_c. The contributions of the excited S-wave and P-wave states to the inclusive production of B_c are 58 and 23%, respectively, and hence significant.

MASTER

*Internet address: cheung@utpapa.ph.utexas.edu

[†]Internet address: yuantc@ucdhep.ucdavis.edu

I. Introduction

Bound states composed of two heavy quarks such as $(c\bar{c})$, $(b\bar{b})$ and $(\bar{b}c)$ mesons, and (ccq), (bbq) and (bcq) baryons (q denotes a light quark) are of interests because they can be produced with sizable rates at the current high energy hadron or e^+e^- colliders. The Standard Model predictions of the production rates of these bound states can therefore be confronted with experimental data.

The direct production of heavy mesons like heavy quarkonia and $(\bar{b}c)$ bound states can provide very interesting tests for perturbative QCD. The production of J/ψ and ψ' [1] at the Tevatron has already raised a lot of theoretical interests in explaining the excess of the experimental data above the lowest order perturbative QCD calculation [2], especially at the large transverse momentum (p_T) region. The ideas of heavy quark and gluon fragmentation [3-7] have successfully been applied to explain the experimental data of the prompt J/ψ production from CDF within a factor of five [8-11]. Various attempts [12-14] using the same fragmentation ideas have also been made to resolve the ψ' surplus problem observed at CDF.

Recently, the preliminary CDF results [15] also showed that the production rates of the $1S$, $2S$, and $3S$ Υ states are in excess of the leading order calculation. While the $\Upsilon(1S)$ and $\Upsilon(2S)$ results can be partly explained by including the fragmentation contribution, the $\Upsilon(3S)$ result showed an excess of about an order of magnitude over the QCD prediction even with the fragmentation contribution included [15]. One subtlety is that the relevant p_T for the fragmentation contribution to dominate should be larger in the bottomonium system than in the charmonium system, such that fragmentation is only valid for $p_T \gtrsim (1\text{-}2)\, m_b$ in the former case. Besides, one has to worry about the very small p_T region because, unlike the charmonium system, the experimental triggering conditions on the muon pair from the bottomonium leptonic decay allow experimentalists to measure the transverse momentum of the bottomonium all the way down to about 0-1 GeV [15]. So to fully understand the p_T spectrum of the bottomonium production, different production mechanisms have to be brought into picture in order to explain the production rates in different p_T regions.

2

DISCLAIMER

Portions of this document may be illegible in electronic image products. Images are produced from the best available original document.

The ($\bar{b}c$) meson system, which is *intermediate* between the J/ψ and Υ families, is also an interesting physical system to study. The mass spectrum of the ($\bar{b}c$) mesons can be predicted reliably from quarkonium potential models [16–18] without introducing any new parameters and their decay constants can be computed using QCD spectrum sum rules [17,18]. We will adopt the Particle Data Group [19] conventions, denoting the $1S$ pseudoscalar ($^1S_0$) and vector meson ($^3S_1$) ($\bar{b}c$) states by B_c and B_c^*, respectively. Higher radially and orbitally excited states are labeled by the standard spectroscopy notation: $n\,^{2S+1}L_J$, where the integer n is the principal quantum number, and L, S, and $J = L + S$ are respectively the orbital angular momentum, total spin, and total angular momentum of the bound state. In the LS coupling scheme, for each principal quantum number n, the spin-singlet and the spin-triplet S-wave ($L = 0$) states are denoted by $^1S_0$ and $^3S_1$, respectively. Those for the P-wave ($L = 1$) and D-wave ($L = 2$) states are denoted by $^1P_1$, ^3P_J ($J = 0, 1, 2$), and $^1D_2$, ^3D_J ($J = 1, 2, 3$), respectively.

According to the results of the potential model calculation [16], the first two sets ($n = 1$ and $n = 2$) of S-wave states, the first ($n = 1$) and probably the entire second set ($n = 2$) of P-wave states, and the first set ($n = 1$) of D-wave states lie below the BD flavor threshold. Since QCD interactions are diagonal in flavors, the annihilation channel of excited ($\bar{b}c$) mesons can only occur through the weak gauge boson (W) exchange and is therefore suppressed relative to the electromagnetic and hadronic transitions to other lower lying states. The excited states below the BD threshold will cascade down into the ground state B_c via emission of photons and/or pions, while the other states above the BD threshold decay rapidly into a pair of B and D mesons. Inclusive production of the B_c meson therefore includes the production of the $n = 1$ and $n = 2$ S-wave and P-wave states, and the $n = 1$ D-wave states.

The production of the S-wave ($^1S_0$ and $^3S_1$) states were first computed exactly to leading order in Ref. [20] at the e^+e^- machine, in particular at the Z resonance. Later, it was realized [5,21] that the complicated formulas in these complete calculations can be simplified by a factorization approach. The dominant contribution in the leading order calculation can

3

be factorized into a short distance piece, which describes the partonic process of the decay of Z into a high energy $b\bar{b}$ pair, and a fragmentation piece describing how the $\bar{b}$ antiquark splits into the two S-wave states. The corresponding fragmentation functions $D_{\bar{b}\to B_c}(z)$ and $D_{\bar{b}\to B_c^*}(z)$, which are independent of the short-distance piece, were shown to be calculable by perturbative QCD at the heavy quark mass scale [5]. Recently, the production of the S-wave states has also been computed at hadronic colliders like the Tevatron and the Large Hadron Collider (LHC) both by a complete $\mathcal{O}(\alpha_s^4)$ calculation [22–24] and by using the simpler fragmentation approach [25,26]. We note that unlike the J/ψ production in hadronic collisions in which the major contribution comes from $g \to \chi_{cJ}$ fragmentation followed by the decay $\chi_{cJ} \to J/\psi + \gamma$ [8–11], the fragmentation diagrams for producing $(\bar{b}c)$ mesons belong to a gauge-invariant subset of the whole set of $\mathcal{O}(\alpha_s^4)$ diagrams, which are the leading-order diagrams for producing $(\bar{b}c)$ mesons in hadronic collisions. It is therefore not clear that the production of $(\bar{b}c)$ mesons in hadronic collisions is dominated by parton fragmentation. However, detailed calculations by Chang *et al.* [22] and by Slabospitsky [23] indicated that the fragmentation approach is valid for the S-wave production at the large transverse momentum region. We will discuss more about this later in the closing section.

In this paper, we study the hadronic production of $(\bar{b}c)$ mesons. We compute the production rates of the S-wave and P-wave $(\bar{b}c)$ mesons at the Tevatron using the fragmentation approach. Intuitively, the dominant production mechanism of the $(\bar{b}c)$ mesons at the large transverse momentum region must arise from the direct fragmentation of the heavy $\bar{b}$ antiquark. The relevant question is whether experiments can probe the transverse momentum region where fragmentation dominates. Unfortunately, to answer this question it also requires a complete $\mathcal{O}(\alpha_s^4)$ calculation for the production of the P-wave states, which is not available at the moment. Here we assume that the fragmentation approach also works for production of the P-wave $(\bar{b}c)$ mesons in the transverse momentum range that is being probed experimentally at the Tevatron. In this work, we do not include the contributions from the D-wave states because the corresponding fragmentation functions have not been calculated.

4

Although the production of the D-wave states is of great interest by themselves, they are not expected to contribute an appreciable amount to the inclusive production of B_c. In the near future, like other heavy quarkonia, the production of $(\bar{b}c)$ mesons at the Tevatron may therefore provide another interesting test for perturbative QCD. Although we will only show our results for the positively charged states $(\bar{b}c)$, all the results presented in this work also hold for the negatively charged states $(b\bar{c})$.

The organization of this paper is as follows. In the next section, we discuss in detail the general procedures to calculate the production cross sections using the fragmentation approach. In Sec. III we present the transverse momentum spectra and the integrated cross sections for the production of S-wave and P-wave $(\bar{b}c)$ states, as well as the inclusive production rate for the B_c meson. Discussions and conclusions are made in Sec. IV. For completeness we also collect all the S-wave and P-wave fragmentation functions at the heavy-quark mass scale in the Appendix.

Before leaving this preamble, we note that a preliminary result from CDF had provided a hint for the B_c existence by looking at the production rate of $J/\psi + \pi$ (a clean event presumably arises from B_c decay) in the mass bin of 6.1–6.4 GeV [27].

II. Inclusive production cross sections in the fragmentation approach

Theoretical calculations of production cross sections in high energy hadronic collisions are based on the idea of factorization. Factorization divides an inclusive or exclusive hadronic production process into a short-distance piece and a long-distance piece. The short-distance piece is perturbatively calculable to any desired accuracy in QCD, while the long-distance piece is in general not calculable within perturbation theory but can be parameterized as phenomenological functions, which can be determined by experiments. The factorization used here for the production of $(\bar{b}c)$ mesons divides the process into the production of a

high energy parton (a $\bar{b}$ antiquark or a gluon) and the fragmentation of this parton into various ($\bar{b}c$) states. The novel feature in our approach, which is due to a recent theoretical development [5,7], is that the relevant fragmentation functions at the heavy quark mass scale can be calculated in perturbative QCD to any desired accuracy. This is easily understood from the fact that the fragmentation of a $\bar{b}$ antiquark into a ($\bar{b}c$) meson involves the creation of a $c\bar{c}$ pair out of the vacuum. The natural scale for this particular hadronization is of order of the mass of the quark pair being created. In our case, this scale is of order m_c, which is considerably larger than Λ_{QCD}. One can therefore calculate reliably the fragmentation functions as an expansion in the strong coupling constant α_s using perturbative QCD.

The production of high energy partons also involves the factorization into the parton distribution functions inside the hadrons and the parton-parton hard scattering. Let H denotes any ($\bar{b}c$) meson states. The differential cross section $d\sigma/dp_T$ versus the transverse momentum p_T of H is given by

$$
\begin{aligned}
\frac{d\sigma}{dp_T}(p\bar{p} \to H(p_T)X) &= \sum_{ij} \int dx_1 dx_2 dz\, f_{i/p}(x_1, \mu) f_{j/\bar{p}}(x_2, \mu) \left[\frac{d\hat{\sigma}}{dp_T}(ij \to \bar{b}(p_T/z)X, \mu) \right. \\
&\left. \times D_{\bar{b} \to H}(z, \mu) + \frac{d\hat{\sigma}}{dp_T}(ij \to g(p_T/z)X, \mu)\, D_{g \to H}(z, \mu) \right] .
\end{aligned}
\tag{1}
$$

The physical interpretation is as follows: a heavy $\bar{b}$ antiquark or a gluon is produced in a hard process with a transverse momentum p_T/z and then it fragments into H carrying a longitudinal momentum fraction z. We assume that H is moving in the same direction as the fragmenting parton. In the above equation, $f_{i/p(\bar{p})}(x, \mu)$'s are the parton distribution functions, $d\hat{\sigma}$'s represent the subprocess cross sections, and $D_{i \to H}(z, \mu)$'s are the parton fragmentation functions at the scale μ. For the production of $\bar{b}$ antiquark, we include the subprocesses $gg \to b\bar{b}$, $g\bar{b} \to g\bar{b}$, and $q\bar{q} \to b\bar{b}$; while for the production of the gluon g, we include the subprocesses $gg \to gg$, $q\bar{q} \to gg$, and $gq(\bar{q}) \to gq(\bar{q})$. In Eq. (1), the factorization scale μ occurs in the parton distribution functions, the subprocess cross sections, and the fragmentation functions. In general, we can choose three different scales for these three entities. For simplicity and ease of estimating the uncertainties due to changes in scale, we

choose a common scale μ for all three of them.

The physical production rates should be independent of choices of the scale μ, because μ is just an artificial entity introduced to factorize the whole process into different parts in the renormalization procedure. However, this independence of scale can only be achieved if both the production of the high energy partons and the fragmentation functions are calculated to all orders in α_s. So far, only the next-to-leading order $\hat{\sigma}$'s and the leading order fragmentation functions are available, so the production cross sections do depend on the choice of μ to a certain degree. We will estimate the dependence on μ by varying the scale $\mu = (0.5 - 2)\mu_R$, where μ_R is our primary choice of scale

$$\mu_R = \sqrt{p_T^2(\text{parton}) + m_b^2} \; . \tag{2}$$

This choice of scale, which is of order $p_T(\text{parton})$, avoids the large logarithms in the short-distance part $\hat{\sigma}$'s. However, we have to sum over the logarithms of order μ_R/m_b in the fragmentation functions. But this can be implemented by evolving the Altarelli-Parisi equations for the fragmentation functions.

II.a   Evolution of Fragmentation Functions

The Altarelli-Parisi evolution equations for the fragmentation functions are

$$\mu\frac{\partial}{\partial\mu}D_{\bar{b}\to H}(z,\mu) = \int_z^1 \frac{dy}{y}P_{\bar{b}\to\bar{b}}(z/y,\mu)\,D_{\bar{b}\to H}(y,\mu) + \int_z^1 \frac{dy}{y}P_{\bar{b}\to g}(z/y,\mu)\,D_{g\to H}(y,\mu)\,, \tag{3}$$

$$\mu\frac{\partial}{\partial\mu}D_{g\to H}(z,\mu) = \int_z^1 \frac{dy}{y}P_{g\to\bar{b}}(z/y,\mu)\,D_{\bar{b}\to H}(y,\mu) + \int_z^1 \frac{dy}{y}P_{g\to g}(z/y,\mu)\,D_{g\to H}(y,\mu)\,, \tag{4}$$

where H denotes any $(\bar{b}c)$ states, and $P_{i\to j}$ are the usual Altarelli-Parisi splitting functions. The leading order expressions for $P_{i\to j}$ can be found in the Appendix.

The boundary conditions for the above Altarelli-Parisi equations are the fragmentation functions $D_{\bar{b}\to H}(z,\mu_0)$ and $D_{g\to H}(z,\mu_0)$ that we can calculate by perturbative QCD at the initial scale μ_0, which is of the order of the b-quark mass. At present, all the S-wave [5] and P-wave [7] fragmentation functions for $\bar{b} \to (\bar{b}c)$ have been calculated to leading order in α_s.

7

They are all collected in the Appendix. The initial scale μ_0 for $D_{\bar{b} \to H}(z, \mu_0)$ is chosen to be $\mu_0 = m_b + 2m_c$, which is the minimum virtuality of the fragmenting $\bar{b}$ antiquark [5]. On the other hand, since the initial gluon fragmentation function $D_{g \to H}(z, \mu_0)$ is suppressed by one extra power of α_s relative to $D_{\bar{b} \to H}(z, \mu_0)$, we simply choose the initial gluon fragmentation function to be $D_{g \to H}(z, \mu_0) = 0$ for $\mu_0 \leq 2(m_b + m_c)$ — the minimum virtuality of the fragmenting gluon [26]. Thus, our boundary conditions are

$$
\begin{aligned}
D_{g \to H}(z, \mu_0) &= 0 \qquad \text{for} \quad \mu_0 \leq 2(m_b + m_c) \,, \\
D_{\bar{b} \to H}(z, \mu_0 = m_b + 2m_c) &= \quad \text{those given in the Appendix.}
\end{aligned}
\tag{5}
$$

We can also examine the relative importance of these fragmentation functions. The initial $D_{\bar{b} \to H}(z, \mu_0)$ is of order α_s^2, whereas the initial $D_{g \to H}(z, \mu_0)$ is of order α_s^3 and has been set to be zero for $\mu_0 \leq 2(m_b + m_c)$ as discussed above. But when the scale is evolved up to a higher scale μ, $D_{\bar{b} \to H}(z, \mu)$ is still of order α_s^2, while the induced $D_{g \to H}(z, \mu)$ is of order $\alpha_s^3 \log(\mu/\mu_0)$. At a sufficiently large scale μ the logarithmic enhancement can offset the extra suppression factor of α_s. Thus the Altarelli-Parisi induced gluon fragmentation functions can be as important as the $\bar{b}$ antiquark fragmentation, even though the initial gluon fragmentation functions are suppressed. While these Altarelli-Parisi induced gluon fragmentation functions play only a moderate role at the Tevatron, they will play a more significant role at the LHC [26].

To obtain the fragmentation functions at an arbitrary scale greater than μ_0, we numerically integrate the Altarelli-Parisi evolution equations (3)–(4) with the boundary conditions given by Eq. (5). Since the initial light-quark fragmentation functions $D_{q \to H}(z, \mu_0)$ are of order α_s^4, one can set them to be zero as well for $\mu_0 \leq 2(m_b + m_c)$. One may ask if the light-quark fragmentation functions can be induced in the same manner as in the gluon case by Altarelli-Parisi evolution. Since both the Altarelli-Parisi splitting functions $P_{q \to q}$ and $P_{q \to g}$ are total plus-functions, the induced light-quark fragmentation functions $D_{q \to H}(z)$ can only be total plus-functions or vanishing identically. We do not anticipate that these induced light-quark fragmentation functions, if nontrivial, will play any significant role in

our analysis.

III. Numerical results

Leading order QCD formulas are employed for the parton-level scattering cross sections and CTEQ(2M) [28] is used for the initial parton distributions. The inputs to the initial fragmentation functions are the heavy quark masses m_b and m_c, and the nonperturbative parameters associated with the wavefunctions of the bound states. For the S-wave states there is only one nonperturbative parameter, which is the radial wavefunction $R_{nS}(0)$ at the origin. However for the P-wave fragmentation functions we have two nonperturbative parameters H_1 and H_8' associated with the color-singlet and the color-octet mechanisms, respectively [29]. Two of the P-wave states ($^1P_1$ and $^3P_1$) are mixed to form the two physical states, denoted by $|1^+\rangle$ and $|1^{+\prime}\rangle$. Further details of the mixings can be found in Refs. [7,16]. The above input parameters for the fragmentation functions are summarized in Table I.

As mentioned in the previous section, we have set the scale μ in the parton distribution functions, subprocess cross sections, and the fragmentation functions to be the same. We will later vary μ between $0.5\mu_R$ and $2\mu_R$, where μ_R is given in Eq. (2), to study the dependence on the choice of scale. For the strong coupling constant $\alpha_s(\mu)$ entered in the subprocess cross sections, we employ the following simple expression

$$\alpha_s(\mu) = \frac{\alpha_s(M_Z)}{1 + \frac{33-2n_f}{6\pi}\,\alpha_s(M_Z)\ln(\frac{\mu}{M_Z})}\,, \tag{6}$$

where n_f is the number of active flavors at the scale μ and $\alpha_s(M_Z) = 0.118$. In order to simulate the detector coverage at the Tevatron, we impose the following acceptance cuts on the transverse momentum and rapidity of the $(\bar{b}c)$ state H:

$$p_T(H) > 6\,\text{GeV} \qquad \text{and} \qquad |y(H)| < 1\,. \tag{7}$$

The numerical results for the p_T spectra for the $(\bar{b}c)$ state H with various spin-orbital quantum numbers are shown in Fig. 1 and Fig. 2 for the cases of principal quantum number

9

$n = 1$ and $n = 2$, respectively. The integrated cross sections versus $p_T^{\min}(H)$ are also shown in Figs. 3 and 4 for the cases of $n = 1$ and $n = 2$, respectively.

Now we can predict the inclusive production rate of the B_c meson. As the annihilation channel is suppressed relative to the electromagnetic/hadronic transitions, all the excited states below the BD threshold will decay subsequently into the ground state B_c via emission of photons or pions. Since the energies of these emitted photons and/or pions are limited by the small mass differences between the initial and final $(\bar{b}c)$ states, the transverse momenta of the $(\bar{b}c)$ mesons are not appreciably affected during the cascades. Therefore, we can simply add up the p_T spectra (Fig. 1 and Fig. 2) of all the states to represent the p_T spectrum of the inclusive B_c production. Similarly, we can add up the integrated cross sections (Fig. 3 and Fig. 4) to represent the integrated cross section for the inclusive B_c production. Thus, we can obtain the inclusive production rate of B_c as a function of $p_T^{\min}(B_c)$. Table II gives the inclusive cross sections for the B_c meson at the Tevatron as a function of $p_T^{\min}(B_c)$, including all the contributions from the $n = 1$ and $n = 2$ S-wave and P-wave states. These cross sections should almost represent the inclusive production of B_c by fragmentation, because the contributions from the D-wave states are expected to be minuscule. The results for $\mu = \mu_R/2$, μ_R, and $2\mu_R$ are also shown. The variation of the integrated cross sections with the scale μ is always within a factor of two, and only about 20% for $p_T > 10$ GeV. We will discuss more about the dependence of scale in the next section.

At the end of Run Ib at the Tevatron, the total accumulated luminosities can be up to 100–150 pb^{-1} or more. With $p_T > 6$ GeV, there are about 5×10^5 B_c^+ mesons. The lifetime of the B_c meson has been estimated to be of order 1–2 picosecond [16], which is long enough to leave a displaced vertex in a silicon vertex detector. Besides, B_c decays into $J/\psi_a + X$ very often, where X can be a π^+, ρ^+, or $\ell^+\nu_l$, and J/ψ can be detected easily through its leptonic decay modes. The inclusive branching ratio of $B_c \to J/\psi + X$ is about 10% [30]. When X is $e^+\nu_e$ or $\mu^+\nu_\mu$, we will obtain the striking signature of three-charged leptons coming off from a common secondary vertex. The combined branching ratio of

10

$B_c \to J/\psi \ell^+ \nu_\ell \to \ell'^+ \ell'^- \ell^+ \nu_\ell$ $(\ell, \ell' = e, \mu)$ is about 0.2%. This implies that there will be of order 10^3 such distinct events for 100 pb^{-1} luminosity at the Tevatron. Even taking into account the imperfect detection efficiencies, there should be enough events for confirmation. However, this mode does not afford the full reconstruction of the B_c. If X is some hadronic states, e.g., pions, the events can be fully reconstructed and the B_c meson mass can be measured. The process $B_c \to J/\psi + \pi^+ \to \ell^+ \ell^- \pi^+$ is likely to be the discovery mode for B_c. Its combined branching ratio is about 0.03%, which implies about 300 such distinct events at the Tevatron with a luminosity of 100 pb^{-1}.

After the next fixed target runs at the Tevatron, the Main Injector will be installed in 1996–1997 according to the present plan [31]. The Main Injector will give a significant boost in the luminosity while the center-of-mass energy stays the same. The upgraded luminosity is estimated to be about ten times larger than its present value. This enables Run II to accumulate a total luminosity of 1–2 fb^{-1}, which implies that about $10^7 - 10^8$ B_c mesons will be produced. With the Main Injector installed, it might be possible to produce the D-wave $(\bar{b}c)$ states with sizable rates.

Tevatron will continue running until the next generation of hadronic colliders, e.g., the LHC. The present design of the LHC is at a center-of-mass energy of 14 TeV and the yearly luminosity is of order 100 fb^{-1}. In Table III, we show the inclusive cross sections for the B_c meson at the LHC as a function of $p_T^{\min}(B_c)$ including the contributions from $n = 1$ and $n = 2$ S-wave and P-wave states. With the assumed 100 fb^{-1} luminosity there are about 3×10^9 B_c mesons with $p_T > 10$ GeV and $|y(B_c)| < 2.5$. With such a high luminosity at LHC, one expects sizable numbers of the various D-wave $(\bar{b}c)$ states to be produced as well. The LHC will then be a copious source of $(\bar{b}c)$ mesons such that their properties e.g., spectroscopy and decays, can be thoroughly studied. In addition, the mixing and CP violation studies are possible. For example, one can use B_c to tag the flavor of B_s in the decay $B_c^+ \to B_s^0 \ell^+ \nu_l$ for the studies of $B_s^0 - \bar{B}_s^0$ mixing. Also, CP violations in the B_c system can be studied by looking at the difference in the partial decay widths of $B_c^+ \to X$ and $B_c^- \to \bar{X}$.

11

IV. Discussions and conclusions

We now briefly discuss the various sources of uncertainties in our calculation. One uncertainty comes from the use of the naive Altarelli-Parisi evolution equations. As pointed out in Refs. [8,32], the naive Altarelli-Parisi equations in Eqs. (3)–(4) do not respect the phase space constraints. Inhomogeneous evolution equations were then advocated to remedy for these problems. The major effect is to correct the unphysical blow-up of the evolved gluon fragmentation functions when z gets too close to 0. The corrected gluon fragmentation functions, instead of the blow-up at $z = 0$, turned to zero smoothly below a certain threshold value of z. Despite the dramatic changes of the evolved gluon fragmentation functions for small z values, this effect will not show up easily in our calculation because the small z region is very likely excluded by the transverse momentum cut imposed on the $(\bar{b}c)$ mesons. Therefore, in this paper we keep on using the homogeneous Altarelli-Parisi equations in Eqs. (3)–(4) to evolve our fragmentation functions.

A second source of uncertainty is due to the choice of the factorization scale μ. We show in Fig. 5 the dependence of the differential cross sections on the factorization scale μ by plotting the results for the various choices of $\mu = \mu_R/2, \mu_R$, and $2\mu_R$. For clarity we only show the curves for the $1\,^1S_0$ and $1\,^3P_0$ states in Fig. 5. The behaviors for other states are similar. Note that in the $\mu = \mu_R/2$, μ_R, and $2\mu_R$ curves, the running scales used in the strong coupling constant α_s, which entered in $d\hat{\sigma}$'s, and in the parton distribution functions $f_i(x)$'s are equal to μ, while the running scale used in the fragmentation functions is set to be max (μ, μ_0), where μ_0 is the prescribed initial scale for the fragmentation functions defined in Eq.(5). Figure 5 shows that the change in the factorization scale μ gives different results for the differential cross sections. The $\mu = 2\mu_R$ curves show that the differential cross sections increase (decrease) only slightly at the low (high) p_T region. Although the $\mu = \mu_R/2$ curves demonstrate larger changes in the differential cross sections, the variations are always within a factor of two. The integrated cross sections at various $p_T^{\min}(B_c)$, as already shown in Table II, also indicate lesser sensitivity in the scale as one increases $p_T^{\min}(B_c)$. The

variations of differential cross sections with the scale μ demonstrate the effects of the next-to-leading order (NLO) corrections. Only if all the NLO corrections are calculated for each piece contained in Eq. (1), namely the parton distribution functions, the parton-parton hard scattering cross sections, and the fragmentation functions, can these variations be reduced substantially. Since the perturbative QCD fragmentation functions are only calculated to leading order, the NLO calculations of the perturbative QCD fragmentation functions can provide an improvement to our calculation. However, due to the rather weak dependence on the scale in our leading order calculation, our results should be rather stable under higher order perturbative corrections.

Other uncertainties come from the input parameters to the boundary conditions of the fragmentation functions. These are the heavy quark masses m_b and m_c, and the nonperturbative parameters describing the bound states. Slight changes in m_c and m_b could possibly lead to appreciable changes in the fragmentation functions, as indicated by the m^3 and m^5 dependence respectively in the denominators of the S-wave and P-wave fragmentation functions. (Note that $H_1/m \approx 9|R'(0)|^2/(32\pi m^5)$.) However, in the numerators the wavefunctions at the origin $|R(0)|^2$ and $|R'(0)|^2$ also scale like m^3 and m^5, respectively. Therefore the dependence on the heavy quark masses should be mild in the fragmentation functions. Although the color-octet parameters H_8''s are not well determined, they do not play a significant role in the present context.

Finally, we discuss the controversy in recent literature [22–24] concerning about the importance of parton fragmentation in the production of the B_c (B_c^*) meson at hadronic colliders. The controversy arises because the Feynman diagrams responsible for the $\bar{b}$ antiquark fragmentation belong to a gauge-invariant subset of the whole set of Feynman diagrams, which contribute at the order of α_s^4. Thus, there is a competition between the fragmentation contribution and the non-fragmentation contribution, which some authors called recombination. So far, three independent groups [22–24] have presented such a complete $\mathcal{O}(\alpha_s^4)$ calculation. Chang *et al.* [22] and Slabospitsky [23] agreed that the fragmentation contribu-

tion dominates at the large transverse momentum region. However, we could not find in their work the precise value of p_T at which the fragmentation contribution begins to dominate. On the other hand, Berezhnoy et al. [24] claimed that fragmentation never dominates for all kinematical region of p_T and the recombination diagrams can never be ignored.

Slabospitsky's and Berezhnoy et al.'s results were roughly consistent with each other, even though their input parameters were somehow different. Slabospitsky used a B_c decay constant $f_{B_c} = 510$ MeV and studied the scale sensitivity in the cross sections by evaluating the strong coupling constant α_s and the parton distribution functions at three different scales $\hat{s}$, $\hat{s}/4$, and $(2M_{B_c})^2$, where $\hat{s}$ is the invariant mass squared of the parton-parton scattering. On the other hand, Berezhnoy et al. used a $f_{B_c} = 570$ MeV and a fixed value of $\alpha_s = 0.2$ but did not mention explicitly at what scale they evaluated the parton distribution functions. We estimate that the difference between these two calculations in terms of total cross sections of B_c was within a factor of 2. Surprisingly, their results were much larger than that obtained by Chang et al., who used a $f_{B_c} = 480$ MeV and evaluated α_s and the parton distribution functions at the scale $\hat{s}/4$. Chang et al. had a total B_c cross section at least 10 times smaller than Slabospitsky's. This large discrepancy cannot be accounted for by the different choices in the scales of the strong coupling constant or the parton distribution functions.

Our results, depending on the fragmentation approach, are only valid in the large p_T region, because in the low p_T region both the fragmentation and recombination contributions are equally important. Although we cannot compare our integrated cross sections of B_c and B_c^* with the exact $\mathcal{O}(\alpha_s^4)$ calculations, we can compare the shape of the p_T spectra for $p_T > 6$ GeV. We compare our results with those obtained by Chang and Chen [22] and Slabospitsky [23]. We note that our p_T spectrum for the $1\,^1S_0$ state shown in Fig. 1 has about the same slope as the corresponding one in Fig.2 of Chang and Chen and in Fig.4a of Slabospitsky. However, the overall normalization of our curve is about 3–4 times larger than Chang and Chen's and about 1/3 of Slabospitsky's. The discrepancy in overall normalization between our result and Slabospitsky's can be explained by (i) we have imposed

14

a rapidity cut of $|y(B_c)| < 1$ while Slabospitsky did not, (ii) we used a smaller decay constant $f_{B_c} = 495$ MeV, and (iii) we only counted the positively charged state while Slabospitsky had counted both charges. We also note that in view of a recent calculation [33] of the QCD correction to the decay constant f_{B_c}, perhaps a smaller value of f_{B_c} is preferred. However, we cannot explain the discrepancy in the overall normalization between our result and Chang et al.'s. Another difference is that in our fragmentation approach, we have also included the subprocess $g\bar{b} \to g\bar{b}$ followed by the $\bar{b}$ fragmentation, while this contribution was not considered in the exact perturbative QCD calculations.

Despite the disagreement among the three sets of complete $\mathcal{O}(\alpha_s^4)$ calculations, we can still draw the following conclusion. Since the slope of our p_T curve for B_c is similar to that obtained from the complete $\mathcal{O}(\alpha_s^4)$ calculations, we believe that the fragmentation contribution should begin to dominate the production of $(\bar{b}c)$ mesons at $p_T \gtrsim 10$ GeV. Also, we would like to emphasize that the detector coverage and performance do require a minimum transverse momentum cut and a rapidity cut on the B_c meson. Thus, the non-fragmentation (recombination) contribution, which is substantial at low p_T, becomes less important as the lowest p_T range is being excluded.

In this paper, we have performed calculations of the transverse momentum spectra and integrated cross sections for the S- and P-wave $(\bar{b}c)$ mesons. We have also predicted the inclusive production rate for the B_c meson, and found that there should be enough signature events to confirm the existence of B_c at the Tevatron, whereas the LHC will be a copious source of B_c. Nevertheless, one should keep in mind that what we have calculated in this paper represents only the contribution from fragmentation, while there should also be other non-fragmentation contributions, especially at the low p_T region ($p_T \lesssim 10$ GeV). At least, our results represent a lower bound of the production rate for B_c. In the near future, the production of B_c at the Tevatron would provide another interesting test for perturbative QCD, and we expect a very exciting experimental program of B_c at the LHC.

15

Acknowledgement

Appendix

The Altarelli-Parisi evolution equations were given in Eqs. (3)-(4). For convenience, we also list all the Altarelli-Parisi kernels in the following,

$$P_{\bar{b}\to\bar{b}}(x,\mu) = \frac{4\alpha_s(\mu)}{3\pi}\left(\frac{1+x^2}{1-x}\right)_+, \tag{A.1}$$

$$P_{\bar{b}\to g}(x,\mu) = \frac{4\alpha_s(\mu)}{3\pi}\left(\frac{1+(1-x)^2}{x}\right)_+, \tag{A.2}$$

$$P_{g\to\bar{b}}(x,\mu) = \frac{\alpha_s(\mu)}{2\pi}\left(x^2+(1-x)^2\right), \tag{A.3}$$

$$P_{g\to g}(x,\mu) = \frac{6\alpha_s(\mu)}{\pi}\left(\frac{x}{(1-x)_+}+\frac{1-x}{x}+x(1-x)+\left(\frac{11}{12}-\frac{n_f}{18}\right)\delta(1-x)\right), \tag{A.4}$$

where n_f is the number of active flavors below the scale μ.

The fragmentation functions $D_{\bar{b}\to H}(z,\mu_0)$ for the S-wave and P-wave $(\bar{b}c)$ states have been obtained to leading order in strong coupling constant α_s at the heavy quark mass scale $\mu_0 = m_b + 2m_c$. We introduce the following notations: $r = m_c/(m_b + m_c)$, $\bar{r} = 1 - r$, and $m = m_b m_c/(m_b + m_c)$. The nonperturbative parameters are $R_{nS}(0)$ for the S-wave states, and $H_1(n)$ and $H'_8(n)$ for the P-wave states. The mixing angle between the $^1P_1$ and $^3P_1$ states is denoted by $\cos\theta_{\text{mix}}$. The numerical values of these input parameters can be inferred from potential model calculations (see for example [16]) and are listed in Table I for convenience. The scale of the strong coupling constant entered in $D_{\bar{b}\to H}(z,\mu_0)$ is set to be $2m_c$.

The S-wave fragmentation functions are [5]

$$\begin{aligned}
D_{\bar{b}\to\bar{b}c(n^1S_0)}(z,\mu_0) &= \frac{2\alpha_s(2m_c)^2|R_{nS}(0)|^2}{81\pi m_c^3}\frac{rz(1-z)^2}{(1-\bar{r}z)^6}\\
&\times\left[6 - 18(1-2r)z + (21-74r+68r^2)z^2\right.\\
&\left. - 2\bar{r}(6-19r+18r^2)z^3 + 3\bar{r}^2(1-2r+2r^2)z^4\right],
\end{aligned}$$
$$\tag{A.5}$$

17

$$
D_{\bar{b}\to\bar{b}c(n^3S_1)}(z,\mu_0) = \frac{2\alpha_s(2m_c)^2|R_{nS}(0)|^2}{27\pi m_c^3}\frac{rz(1-z)^2}{(1-\bar{r}z)^6}
$$

$$
\times\ \Big[\,2\ -\ 2(3-2r)z\ +\ 3(3-2r+4r^2)z^2\ -\ 2\bar{r}(4-r+2r^2)z^3
$$

$$
+\ \bar{r}^2(3-2r+2r^2)z^4\Big]\ . \tag{A.6}
$$

Polarized S-wave fragmentation functions can also be found in Ref. [34] but they are not used in this work.

The P-wave fragmentation functions consist of two terms, the color-singlet piece (H_1 term) and the color octet piece (H_8' term) [7]:

$$
D_{\bar{b}\to\bar{b}c(n^1P_1)}(z,\mu_0) = \frac{H_{1(\bar{b}c)}(n)}{m}D^{(1)}_{\bar{b}\to\bar{b}c(^1P_1)}(z,\Lambda) + 3\frac{H'_{8(\bar{b}c)}(\Lambda)}{m}D^{(8)}_{\bar{b}\to\bar{b}c(^1S_0)}(z)\ , \tag{A.7}
$$

$$
D_{\bar{b}\to\bar{b}c(n^3P_J)}(z,\mu_0) = \frac{H_{1(\bar{b}c)}(n)}{m}D^{(1)}_{\bar{b}\to\bar{b}c(^3P_J)}(z,\Lambda) + (2J+1)\frac{H'_{8(\bar{b}c)}(\Lambda)}{m}D^{(8)}_{\bar{b}\to\bar{b}c(^3S_1)}(z)\ ,
$$

$$
\tag{A.8}
$$

where Λ is a factorization scale for the P-wave fragmentation functions. It separates the reduced heavy quark mass scale m and the scale mv which characterizes the bound state structures with v being the typical relative velocity of the heavy quark and antiquark inside the bound state. In our numerical work, we will choose $\Lambda \sim m$.

At leading order the color-singlet pieces do not depend on Λ and they are given by

$$
D^{(1)}_{\bar{b}\to\bar{b}c(^1P_1)}(z) = \frac{16\alpha_s^2(2m_c)}{243}\frac{r\bar{r}^3z(1-z)^2}{(1-\bar{r}z)^8}\Big[6 - 6(4r^2 - 8r + 5)z
$$

$$
+\ (32r^4 - 96r^3 + 250r^2 - 210r + 69)z^2
$$

$$
+\ 8\bar{r}(4r^4 + 12r^3 - 48r^2 + 37r - 12)z^3
$$

$$
+\ 2\bar{r}^2(16r^4 + 161r^2 - 114r + 42)z^4 - 6\bar{r}^3(4r^3 + 28r^2 - 15r + 7)z^5
$$

$$
+\ \bar{r}^4(46r^2 - 14r + 9)z^6\Big]\ , \tag{A.9}
$$

$$
\begin{aligned}
D^{(1)}_{\bar{b}\to\bar{b}c(^3P_0)}(z) &= \frac{16\alpha_s^2(2m_c)}{729}\frac{r\bar{r}^3z(1-z)^2}{(1-\bar{r}z)^8}\Bigg[6(4r-1)^2+6(4r-1)(20r^2-16r+5)z \\
&+ (832r^4-1456r^3+1058r^2-362r+63)z^2 \\
&- 8\bar{r}(100r^4-184r^3+118r^2-22r+9)z^3 \\
&+ 2\bar{r}^2(416r^4-776r^3+369r^2+42r+24)z^4 \\
&- 2\bar{r}^3(240r^4-516r^3+232r^2+59r+9)z^5 \\
&+ \bar{r}^4(96r^4-240r^3+134r^2+34r+3)z^6\Bigg],
\end{aligned}
\tag{A.10}
$$

$$
\begin{aligned}
D^{(1)}_{\bar{b}\to\bar{b}c(^3P_1)}(z) &= \frac{32\alpha_s^2(2m_c)}{243}\frac{r\bar{r}^3z(1-z)^2}{(1-\bar{r}z)^8}\Bigg[6+6(4r-5)z \\
&+ (16r^4+64r^2-98r+63)z^2+8\bar{r}(2r^4+2r^3-13r^2+11r-9)z^3 \\
&+ 2\bar{r}^2(8r^4-16r^3+47r^2-18r+24)z^4+2\bar{r}^3(8r^3-24r^2+r-9)z^5 \\
&+ \bar{r}^4(12r^2+2r+3)z^6\Bigg],
\end{aligned}
\tag{A.11}
$$

and

$$
\begin{aligned}
D^{(1)}_{\bar{b}\to\bar{b}c(^3P_2)}(z) &= \frac{64\alpha_s^2(2m_c)}{729}\frac{r\bar{r}^5z(1-z)^2}{(1-\bar{r}z)^8}\Bigg[12+12(2r-5)z \\
&+ (92r^2-76r+135)z^2+4(10r^3-54r^2+31r-45)z^3 \\
&+ 2(46r^4-16r^3+123r^2-78r+75)z^4 \\
&- 4\bar{r}(6r^4+9r^3+40r^2-13r+18)z^5 \\
&+ \bar{r}^2(12r^4-12r^3+55r^2-10r+15)z^6\Bigg].
\end{aligned}
\tag{A.12}
$$

The $^1P_1$ and $^3P_1$ states are mixed in general, giving rise to the following physical mass eigenstates $|1^{+'}\rangle$ and $|1^+\rangle$,

$$
|1^{+'}\rangle = \cos\theta_{\mathrm{mix}}|^1P_1\rangle - \sin\theta_{\mathrm{mix}}|^3P_1\rangle,
\tag{A.13}
$$

$$
|1^+\rangle = \sin\theta_{\mathrm{mix}}|^1P_1\rangle + \cos\theta_{\mathrm{mix}}|^3P_1\rangle.
\tag{A.14}
$$

19

Thus, in general, we have

$$
\begin{aligned}
D^{(1)}_{\bar{b}\to\bar{b}c(1+')}(z) &= \cos^2\theta_{\text{mix}} D^{(1)}_{\bar{b}\to\bar{b}c(^1P_1)}(z) + \sin^2\theta_{\text{mix}} D^{(1)}_{\bar{b}\to\bar{b}c(^3P_1)}(z) \\
&\quad - \sin\theta_{\text{mix}}\cos\theta_{\text{mix}} D^{(1)}_{\text{mix}}(z) , \qquad (A.15)
\end{aligned}
$$

$$
\begin{aligned}
D^{(1)}_{\bar{b}\to\bar{b}c(1+)}(z) &= \sin^2\theta_{\text{mix}} D^{(1)}_{\bar{b}\to\bar{b}c(^1P_1)}(z) + \cos^2\theta_{\text{mix}} D^{(1)}_{\bar{b}\to\bar{b}c(^3P_1)}(z) \\
&\quad + \sin\theta_{\text{mix}}\cos\theta_{\text{mix}} D^{(1)}_{\text{mix}}(z) , \qquad (A.16)
\end{aligned}
$$

with

$$
\begin{aligned}
D^{(1)}_{\text{mix}}(z) &= -\frac{32\sqrt{2}\alpha_s^2(2m_c)}{243}\frac{r\bar{r}^3 z(1-z)^2}{(1-\bar{r}z)^6}\Bigg[6 - 6(2r^2 - 4r + 3)z \\
&\quad + (24r^3 + 52r^2 - 52r + 21)z^2 + 2\bar{r}(14r^3 - 6r^2 + 15r - 6)z^3 \\
&\quad - \bar{r}^2(2r^2 + 8r - 3)z^4\Bigg] . \qquad (A.17)
\end{aligned}
$$

Finally, the color-octet pieces are given by

$$
\begin{aligned}
D^{(8)}_{\bar{b}\to\bar{b}c(^1S_0)}(z) &= \frac{\alpha_s^2(2m_c)}{162}\frac{r\bar{r}^3 z(1-z)^2}{(1-\bar{r}z)^6}\Bigg[6 - 18(1-2r)z + (21 - 74r + 68r^2)z^2 \\
&\quad - 2\bar{r}(6 - 19r + 18r^2)z^3 + 3\bar{r}^2(1 - 2r + 2r^2)z^4\Bigg] , \qquad (A.18)
\end{aligned}
$$

and

$$
\begin{aligned}
D^{(8)}_{\bar{b}\to\bar{b}c(^3S_1)}(z) &= \frac{\alpha_s^2(2m_c)}{162}\frac{r\bar{r}^3 z(1-z)^2}{(1-\bar{r}z)^6}\Bigg[2 - 2(3-2r)z + 3(3 - 2r + 4r^2)z^2 \\
&\quad - 2\bar{r}(4 - r + 2r^2)z^3 + \bar{r}^2(3 - 2r + 2r^2)z^4\Bigg] . \qquad (A.19)
\end{aligned}
$$

References

[1] F. Abe *et al.* (CDF Coll.), Phys. Rev. Lett. **69**, 3704 (1992).

[2] E. W. N. Glover, A. D. Martin, and W. J. Stirling, Z. Phys. **C38**, 473 (1988).

[3] E. Braaten and T. C. Yuan, Phys. Rev. Lett. **71**, 1673 (1993).

[4] E. Braaten, K. Cheung, and T. C. Yuan, Phys. Rev. **D48**, 4230 (1993).

[5] E. Braaten, K. Cheung, and T. C. Yuan, Phys. Rev. **D48**, R5049 (1993).

[6] E. Braaten and T. C. Yuan, Phys. Rev. **D50**, 3176 (1994).

[7] T. C. Yuan, Phys. Rev. **D50**, 5664 (1994).

[8] E. Braaten, M. Doncheski, S. Fleming, and M. Mangano, Phys. Lett. **B333**, 548 (1994).

[9] M. Cacciari and M. Greco, Phys. Rev. Lett. **73**, 1586 (1994).

[10] D. P. Roy and K. Sridhar, Phys. Lett. **B339**, 141 (1994).

[11] P. Cho, M. Wise, and S. Trivedi, Caltech preprint CALT-68-1943, hep-ph/9408352 (August 1994).

[12] F. E. Close, Rutherford preprint RAL-94-093, hep-ph/9409203 (September 1994).

[13] P. Cho and M. Wise, Caltech preprint CALT-68-1962, hep-ph/9411303 (November 1994).

[14] E. Braaten and S. Fleming, Northwestern University preprint NUHEP-TH-94-26, hep-ph/9411365 (December 1994).

[15] Talk given by A. Papadimitriou (CDF Coll.), FERMILAB-CONF-94-221-E, contribution to DPF'94 meeting at Albuquerque, NM (August 1994).

[16] E. Eichten and C. Quigg, Phys. Rev. **D49**, 5845 (1994), and references therein.

[17] E. Bagan, H. G. Dosch, P. Gosdzinsky, S. Narison, and J.-M. Richard, Z. Phys. **C64**, 57 (1994).

[18] V. V. Kiselev, A. K. Likhoded, and A. V. Tkabladze, Serpukhov preprint IFVE-94-51, hep-ph/9406339 (April 1994).

[19] Particle Data Group, Phys. Rev. **D50**, 1323 (1994).

[20] L. Claveli, Phys. Rev. **D26**, 1610 (1982); C.-H. Chang and Y.-Q. Chen, Phys. Rev. **D46**, 3845 (1993); Phys. Lett. **B284**, 127 (1992); V. V. Kiselev, A. K. Likhoded, and M. V. Shevlyagin, Z. Phys. **C63**, 77 (1994).

[21] C.-H. Chang and Y.-Q. Chen, Phys. Lett. **B284**, 127 (1992); Phys. Rev. **D46**, 3845 (1992), **D50**, 6013 (1994); Y.-Q. Chen, Phys. Rev. **D48**, 5158 (1993), **D50**, 6013 (1994).

[22] C.-H. Chang and Y.-Q. Chen, Phys. Rev. **D48**, 4086 (1993); C.-H. Chang, Y.-Q. Chen, G.-P. Han, and H.-T. Jiang, Beijing preprint AS-ITP-94-24, hep-ph/9408242 (August 1994).

[23] S. R. Slabospitsky, Serpukhov preprint IFVE-94-53, hep-ph/9404346 (April 1994).

[24] A. V. Berezhnoy, A. K. Likhoded, and M. V. Shevlyagin, Serpukhov preprint IFVE-94-48, hep-ph/9408284 (March 1994).

[25] K. Cheung, Phys. Rev. Lett. **71**, 3413 (1993).

[26] K. Cheung and T. C. Yuan, Phys. Lett. **B325**, 481 (1994).

[27] Todd Niimi (Private communication).

[28] CTEQ Collaboration, J. Botts *et al.*, Phys. Lett. **B304**, 159 (1993).

[29] G. T. Bodwin, E. Braaten, and G. P. Lepage, Argonne Report No. ANL-HEP-PR-94-24, hep-ph/9407339 (July 1994).

[30] A. K. Likhoded, S. R. Slabospitsky, M. Mangano, and G. Nardulli, Nucl. Instrum. Methods **A333**, 209 (1993), and references therein.

[31] Talk given by G. Jackson at the Beyond the Standard Model IV Conference, Tahoe City, CA (December 13-18, 1994).

[32] E. Braaten, K. Cheung, S. Fleming, and T. C. Yuan, Fermilab preprint FERMILAB-PUB-94-305-T, hep-ph/9409316 (September 1994), to appear in Phys. Rev. **D**.

[33] E. Braaten and S. Fleming, Northwestern University preprint, NUHEP-TH-95-1, hep-ph/9501296 (January 1995).

[34] K. Cheung and T. C. Yuan, Phys. Rev. **D50**, 3181 (1994).

Table I: Input parameters to the perturbative QCD fragmentation functions for $n = 1$ and $n = 2$.

	$n = 1$	$n = 2$
m_b	4.9 GeV	4.9 GeV
m_c	1.5 GeV	1.5 GeV
$R_{nS}(0)$	1.28 GeV$^{3/2}$	0.99 GeV$^{3/2}$
H_1	10 MeV	14 MeV
$H_8'(m)$	1.3 MeV	1.8 MeV
$\cos\theta_{\mathrm{mix}}$	0.999	0.957

Table II: The inclusive production cross sections for the B_c meson at the Tevatron including the contributions from all the S-wave and P-wave states below the BD threshold as a function of $p_T^{\mathrm{min}}(B_c)$. The acceptance cuts are $p_T(B_c) > 6$ GeV and $|y(B_c)| < 1$.

p_T^{min} (GeV)	σ (nb)		
	$\mu = \frac{1}{2}\mu_R$	$\mu = \mu_R$	$\mu = 2\mu_R$
6	2.81	5.43	6.93
10	0.87	1.16	1.22
15	0.26	0.29	0.26
20	0.098	0.097	0.083
30	0.021	0.018	0.014

Table III: The inclusive production cross sections for the B_c meson at the LHC including the contributions from all the S-wave and P-wave states below the BD threshold as a function of $p_T^{\min}(B_c)$. The acceptance cuts are $p_T(B_c) > 10$ GeV and $|y(B_c)| < 2.5$.

$p_T^{\min}$ (GeV)	σ (nb), $\mu = \mu_R$
10	33.8
20	4.4
30	1.1
40	0.41

Figure Captions

1. The differential cross section $d\sigma/p_T$ versus p_T of the $(\bar{b}c)$ meson (H) in various spin-orbital states with $n = 1$ at the Tevatron. The acceptance cuts are $p_T(H) > 6$ GeV and $|y(H)| < 1$.

2. Same as Fig.1 for $n = 2$.

3. The integrated cross section $\sigma(p_T > p_T^{\min})$ versus the minimum $p_T^{\min}$ cut on the $(\bar{b}c)$ meson (H) in various spin-orbital states with $n = 1$ at the Tevatron. The acceptance cuts are the same as Fig.1.

4. Same as Fig.3 for $n = 2$.

5. The comparison of the differential cross sections $d\sigma/dp_T$ at different factorization scales for the $1\,^1S_0$ and $1\,^3P_0$ states at the Tevatron. The acceptance cuts are the same as Fig.1.
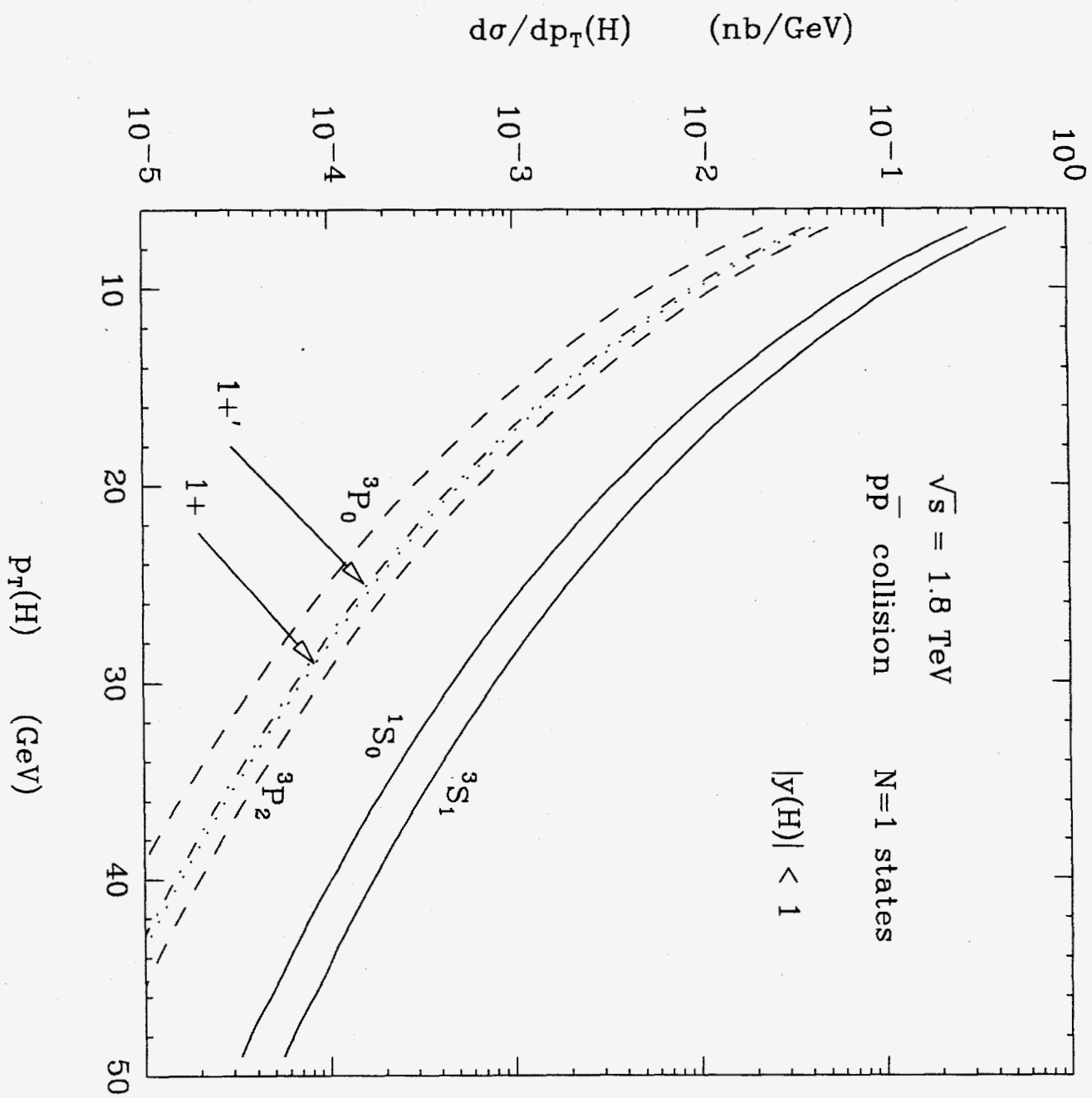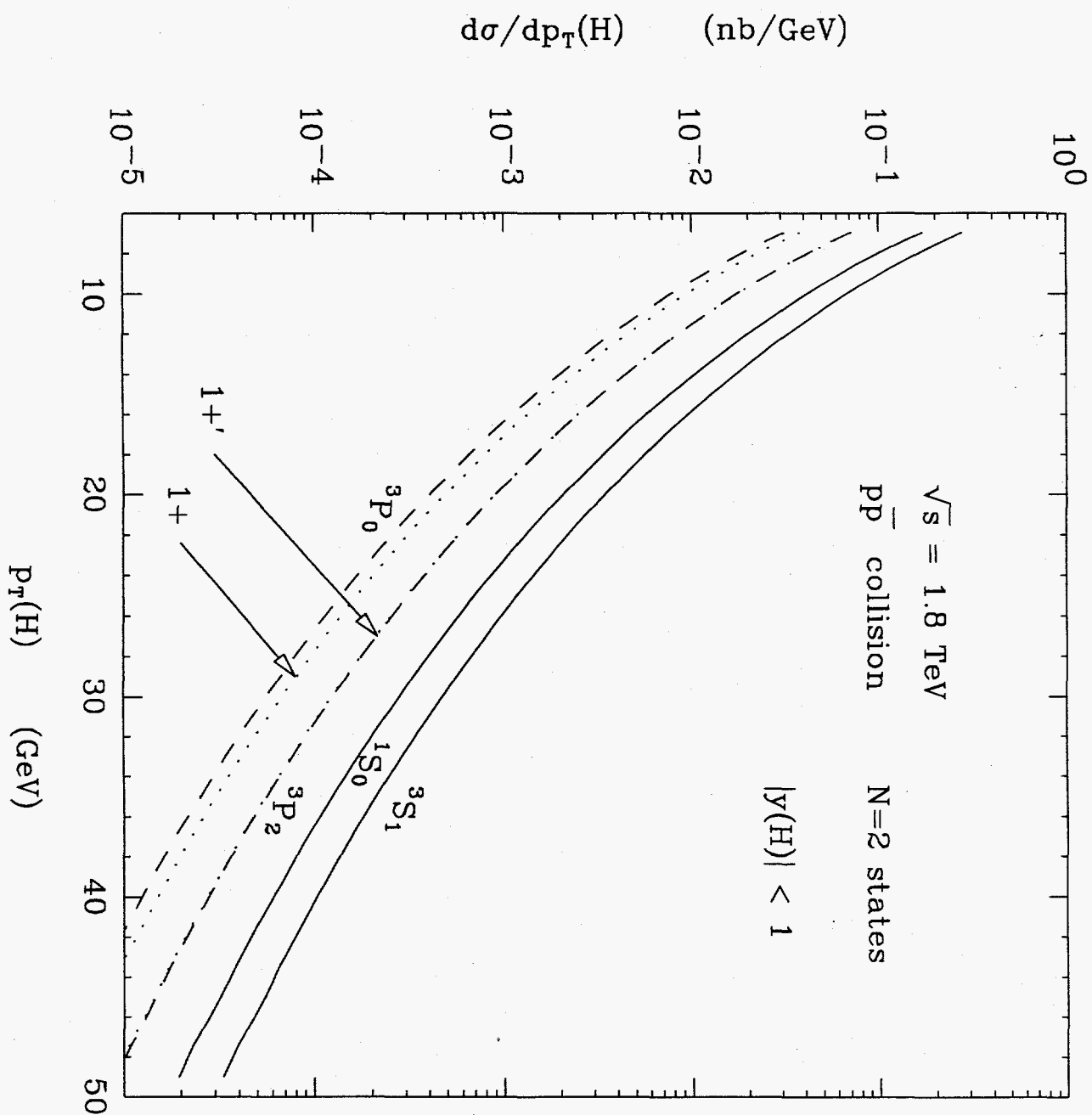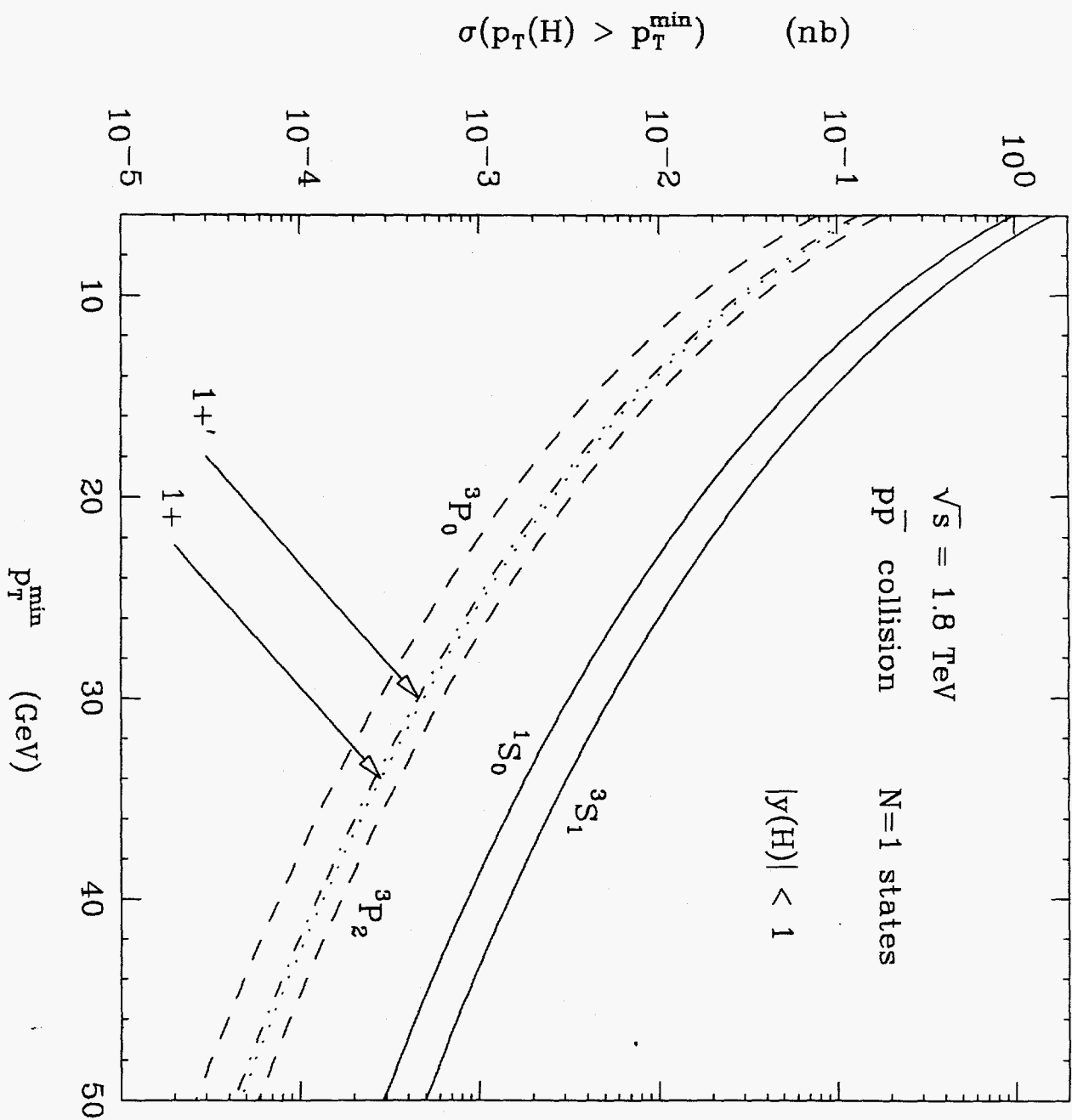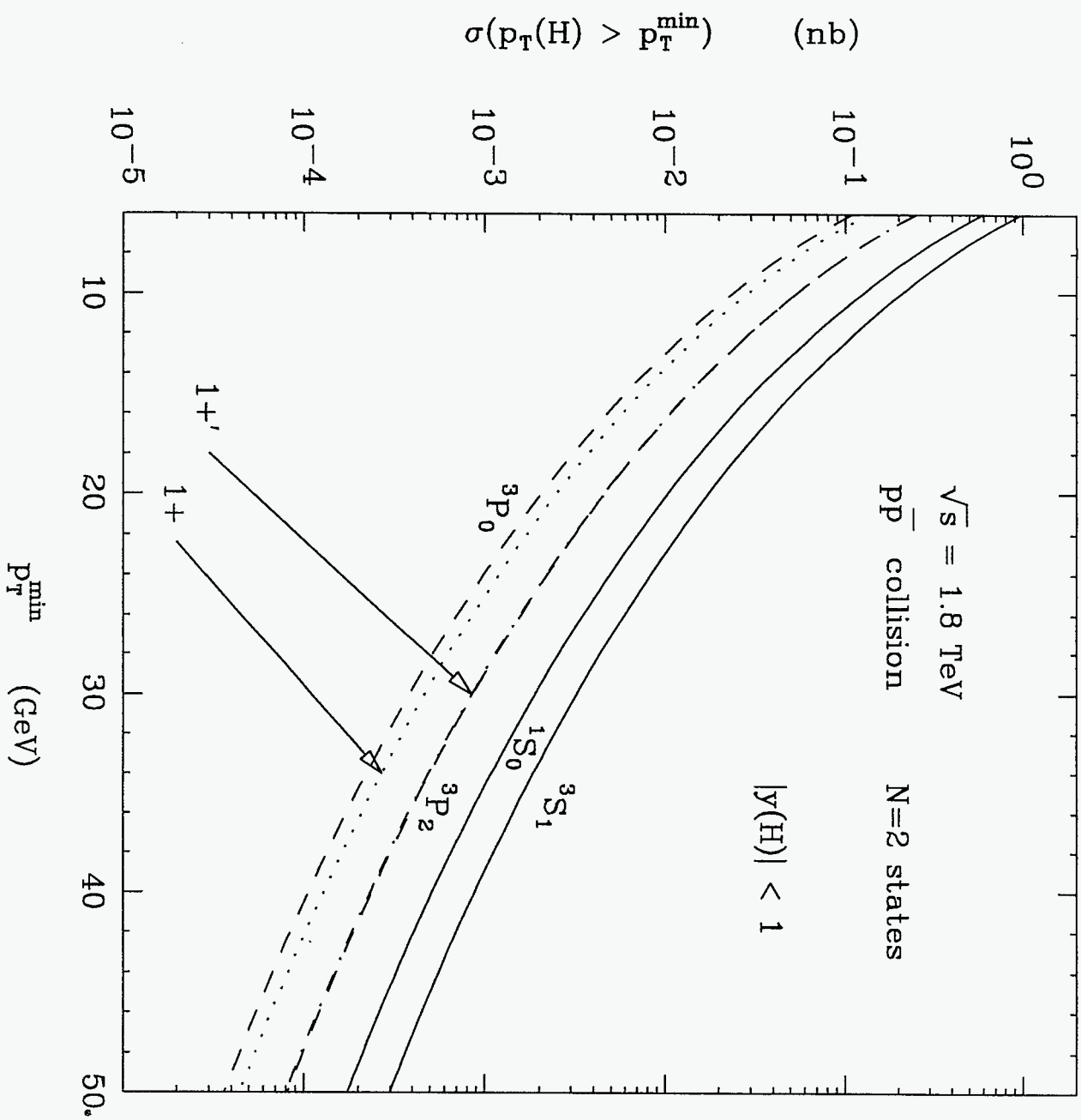
Fig. 1

Fig. 2

$\sigma(p_T(H) > p_T^{min})$ (nb)

$\sqrt{s} = 1.8$ TeV
$p\bar{p}$ collision   N=1 states
$|y(H)| < 1$

$^3P_0$

$1+'$

$1+$

$^1S_0$

$^3S_1$

$^3P_2$

p_T^{min} (GeV)

Fig. 3

Fig. 4

$d\sigma/dp_T(H)$ (nb/GeV)

10^0

10^{-1}

10^{-2}

10^{-3}

10^{-4}

10^{-5}

10   20   30   40   50

$p_T(H)$ (GeV)

$\sqrt{s} = 1.8$ TeV

$p\bar{p}$ collision   N=1 states

$|y(H)| < 1$

$\mu = \mu_R$

$\mu = 2\mu_R$

$\mu = \mu_R/2$

$^3P_0$

$^1S_0$

Fig. 5